International Journal of Heat and Fluid Flow 33 (2012) 182–192

Contents lists available at SciVerse ScienceDirect

International Journal of Heat and Fluid Flow

journal homepage: www.elsevier.com/locate/ijhff

High rotation number effect on heat transfer in a trailing edge channel with tapered ribs

Yao-Hsien Liu [a,*], Michael Huh [b], Je-Chin Han [c]

[a] Department of Mechanical Engineering, National Chiao-Tung University, Hsinchu 30010, Taiwan
[b] Department of Mechanical Engineering, The University of Texas at Tyler, 3900 University Blvd., Tyler, TX 75799, USA
[c] Department of Mechanical Engineering, Texas A&M University, College Station, TX 77843, USA

ARTICLE INFO

Article history:
Received 5 August 2010
Received in revised form 3 October 2011
Accepted 4 October 2011
Available online 1 November 2011

Keywords:
Heat transfer
Gas turbine
Internal cooling
High rotation number
Rib

ABSTRACT

Detailed heat transfer measurements were conducted in a wedge-shaped channel with lateral flow ejection, which is commonly found in the trailing edge cooling cavities of the gas turbine blade. Tapered ribs were applied on the leading and trailing surfaces to enhance heat transfer. Rib spacing (P/e_{max}) was 8 and the ratio of rib height to channel height (e/H) was 0.125. The inlet Reynolds number ranged from 10,000 to 40,000. At the highest rotational speed of 400 rpm, the inlet rotation number was 0.8. Effect of flow ejection on pressure drop, mass flow rate and heat transfer distribution were investigated. Results show that the configuration of this tapered rib enhances heat transfer on the ribbed surface but ejection still has pronounced effects on heat transfer distribution. The experimental data has been correlated with the high rotation number and high buoyancy parameter in ranges similar to industry applications.

1. Introduction

Modern gas turbine engines operate at higher temperatures to reach higher efficiency. Appropriate cooling schemes are required to protect the turbine hot gas path components. Han et al. (2000) provides a comprehensive review of cooling technologies for the gas turbine blade. Internal cooling techniques are commonly used by passing compressed air through cooling cavities inside blade structure as shown in Fig. 1. The geometry of the internal cooling channel needs to fit the profile of the blade. Wide rectangular, wedge, or trapezoidal shaped channels are commonly used to simulate the trailing edge region. Studies have considered low-aspect-ratio rectangular channels with ribs by Griffith et al. (2002) as heat transfer enhancement techniques. Wright et al. (2004) proposed using rectangular channels (AR = 4:1 and 8:1) with pin–fins to simulate the internal cooling passage near the trailing edge. They found that pin–fins enhance heat transfer up to 3.8 times compared to the smooth surface. At the trailing edge cavities, there are discrete holes or slots, which are used to dispense coolant from the internal cooling passages. Lau et al. (1989a, 1989b) studied heat transfer and pressure drop in pin fin channels with long and short ejection holes.

In recent years, more realistic design of trapezoidal or wedge-shaped channels has been applied to the trailing edge region. Taslim et al. (1995) studied seven different tapered orthogonal rib turbulators in a trapezoidal channel with and without bleed holes. They showed that the effects of rib geometrical parameters (P/e, e/D_h) were consistent with previously reported data from the circular or rectangular test sections when surface average values are compared. Hwang and Lu (2001) studied the effects of lateral-flow ejection, pin shapes, and flow Reynolds number in a trapezoidal duct. They concluded that the trapezoidal duct with lateral flow ejection has the highest heat transfer and pressure drop. Carcasci et al. (2003) also investigated heat transfer and pressure drop inside wedge-shaped cooling channels with pedestals (long ribs) and pin–fins. Cunha and Chyu (2006) used a liquid crystal technique to obtain heat transfer data inside the wedge-shaped channel with and without discharge through slots or holes. Pin–fin arrays enhanced heat transfer when compared to the smooth channel in their study.

Rotation profoundly affects heat transfer distribution inside rotating cooling channels. For the radially outward flow, heat transfer is enhanced on the trailing surface while decreased on the leading surface. Wagner et al. (1991) discovered that rotation caused heat transfer to increase up to 3.5 times on the trailing surface and decrease up to 40% on the leading surface compared to the smooth tube flow. Johnson et al. (1994) then extended the work to include the impact of channel orientation on the heat transfer distribution in rotating square channels. Research has been directed towards non-rectangular channels for which rotating data is quite limited. Dutta et al. (1996) studied heat transfer inside rotating triangular ducts with two different model orientations. Results

* Corresponding author. Tel.: +886 35712121x55136; fax: +886 35720634.
E-mail address: yhliu@mail.nctu.edu.tw (Y.-H. Liu).

0142-727X/$ - see front matter © 2011 Elsevier Inc. All rights reserved.
doi:10.1016/j.ijheatfluidflow.2011.10.002

Nomenclature

A	projected surface area of a copper plate segment
A_j	cross sectional area of the slot
A_t	cross sectional area of the test section
AR	channel aspect ratio, W:H
Bo_x	local buoyancy parameter, $(\Delta\rho/\rho)_x(Ro_x)^2R_x/D_h$
C_D	discharge coefficient, $\dot{m}_j/(A_j\sqrt{2\rho(P_{in}-P_{exit})})$
D_h	channel hydraulic diameter, $4A_t/P$
G	mass flux, ρV
H	channel height
h	regionally averaged heat transfer coefficient
k	thermal conductivity of the coolant
L	length of the heated portion of the test section
Nu	regionally averaged Nusselt number, hD_h/k
Nu_0	Nusselt number for fully-developed turbulent flow in the smooth tube
Nu_s	Nusselt number under stationary condition
P	perimeter of the test section
P_{in}	pressure at the inlet of the slot
P_{exit}	pressure at the exit of the slot
Pr	Prandtl number of the coolant
Q_{net}	net heat transfer
Q_{loss}	external heat loss
R	mean radius of rotation (from the center of rotation to center of heated channel)
R_x	local radius of rotation (from the center of rotation to local region within heated channel)
Re_x	local Reynolds number, $\rho V_x D_h/\mu$
Re_i	Reynolds number at the inlet of the test section, $\rho V_i D_h/\mu$
Ro_i	inlet rotation number, $\Omega D_h/V_i$
Ro_x	local rotation number, $\Omega D_h/V_x$
$T_{w,x}$	regionally averaged wall temperature
$T_{b,x}$	local coolant bulk temperature
$T_{f,x}$	local film temperature
V	bulk velocity of the coolant in the streamwise direction
V_i	bulk velocity of the coolant at the inlet of the test section
W	channel width
β	angle of channel orientation with respect to the axis of rotation
μ	viscosity of the coolant
ρ	density of the coolant
$(\Delta\rho/\rho)_x$	local coolant-to-wall density ratio, $(T_{w,x}-T_{b,x})/T_{f,x}$
Ω	rotational speed

showed that ribbed surfaces show different characteristics with respect to rotation number dependency compared to smooth surfaces. In recent years, the effect of rotation on heat transfer has been studied at high rotation numbers and realistic Reynolds number ranges in order to approach real engine conditions. The high rotation number research has been carried out in a smooth rectangular channel (AR = 4:1) by Zhou et al. (2004), a rectangular channel (AR = 1:2) with 45° ribs by Liou et al. (2007), a trapezoidal channel with bleed holes by Chang et al. (2008), a wedge-shaped channel by Wright et al. (2008), and a wedge-shaped channel with slot ejection by Liu et al. (2008).

This paper is an extended study from Liu et al. (2008) by modeling the trailing edge cooling cavity with a wedge-shaped channel. Tapered ribs with an angle of attack of 45° were used to enhance heat transfer. With the coolant flow discharging through the slots, the coolant remaining in the cooling passage decreases. The variation of the coolant flow in the channel needs to be determined to investigate the effect on heat transfer enhancement and the effect of rotation. In the current study, (1) the heat transfer and mass flow inside this wedge-shaped channel with and without cross flow effects were compared; (2) regionally averaged heat transfer distribution in the streamwise and spanwise direction was reported; (3) investigation on heat transfer variation due to the complex interaction of tapered rib induced secondary flows with the effects of rotation and slot ejection; (4) correlations for heat transfer enhancement inside this wedge-shaped channel have been developed at high rotation number and high buoyancy parameter.

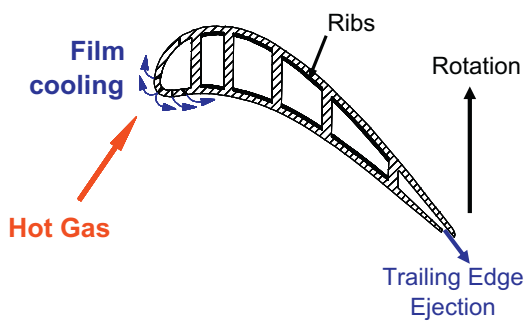

Fig. 1. Gas turbine internal cooling cavities.

2. Experimental setup

2.1. Rotating facility

The rotating heat transfer experiment inside the cooling channel was performed in a rotating facility shown in Fig. 2. Cooling

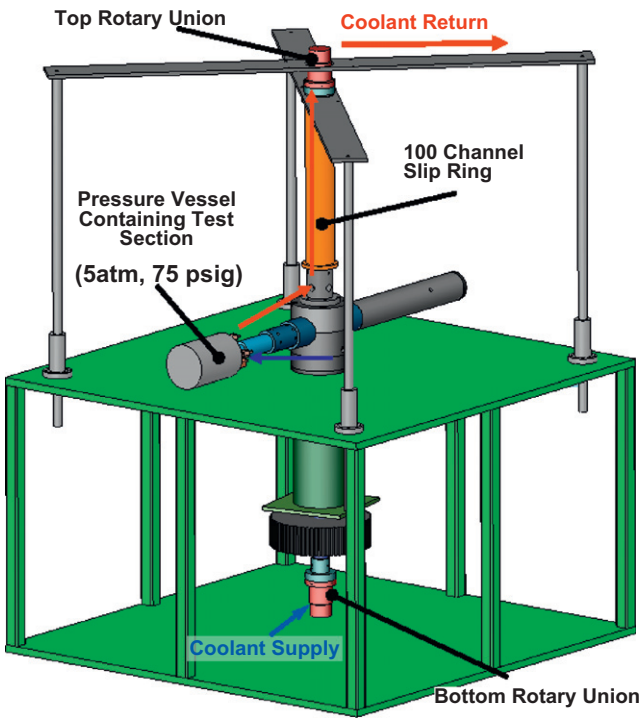

Fig. 2. Rotating facility.

air comes in from the bottom of the facility through a rotary union into a hollow shaft. The air continues to travel through the hub then into the pressure vessel containing the test section. The coolant passes through the heated test section and flows through the copper tubing connected to another rotary union at the top. A gate valve is attached to the pipe to adjust the pressure inside the flow loop. A motor is used to drive the shaft with the frequency controller to control the rotational speed from 0 to 400 rpm. A slip ring with 100 channels is used as an interface to transfer thermocouple signals from the rotating test section to the data acquisition system (Labview). Similarly, current is passed through the slip ring to the test section heaters.

2.2. Wedge-shaped test section

This test section was built to simulate the internal cooling channel with ejection through slots near the trailing edge of a gas turbine. Fig. 3a shows the smooth wedge-shaped test section which has been tested by Liu et al. (2008) previously. In this channel, the cooling air enters the test section through an unheated entrance region with the length of 4.76 cm. Coolant air passes through the heated region with the wedge-shaped cross-section and then discharges through six slots. In order to study the influence of the cross flow effect due to discharged fluid in the second passage, this test section has been modified with removing the portion of the second passage and directing the discharged fluid into the cavity of the pressure vessel as demonstrated in Fig. 3b. For the ribbed case, brass ribs were glued to the leading and trailing surfaces with conductive glue as shown in Fig. 4a. In order to eliminate the heat conduction from adjacent row of copper plates, the tapered ribs were divided into two pieces and the insulation was filled between the ribs. The tapered ribs are in parallel arrangement and staggered on opposite walls. The angle of attack is 45° with a pitch to maximum height ratio (P/e_{max}) of 8. The maximum rib height to hydraulic diameter ratio (e_{max}/D_h) is 0.143 and the rib height to channel height ratio (e/H) is maintained at 0.125. In Fig. 4b, the length of the rib is 4.75 cm with a cross section of 3.18 mm by 3.18 mm on the wide side and a cross section of 3.18 mm by 1.38 mm on the narrow side.

On the leading and trailing surface, each surface was divided into three regions along the spanwise direction – inner, mid-span, and outer regions as shown in Fig. 5. Copper plates were installed on the Garolite CE supporting structure with a 0.159 cm blind hole beneath it for thermocouple instrumentation. The thickness of the copper plate is 0.318 cm. The side wall (close to the middle portion of the blade) is 2.54 cm tall, and the cross-section narrows to 0.32 cm near the trailing edge of the blade as shown in Fig. 6. The distance from the center of rotation to the center of the heated channel is 67.8 cm. The air enters an unheated entrance with a rectangular cross-section of 5.38 cm wide by 3.18 cm tall. The heated length of the channel is 15.56 cm with a hydraulic diameter of 2.25 cm. This gives an overall heated length-to-hydraulic diameter ratio (L/D_h) of 6.30. Six slots were machined near the outer regions as shown in Fig. 6. The width and the length of each slot are 0.16 cm and 1.27 cm, respectively. The distance between each slot is 1.27 cm. The end of this channel is dead ended and all the flow discharges through these six slots into a large pressure vessel then returns to the flow loop. The Reynolds number at the inlet of the channel is controlled from 10,000 to 40,000, each with the rotational speed of 300 rpm and 400 rpm.

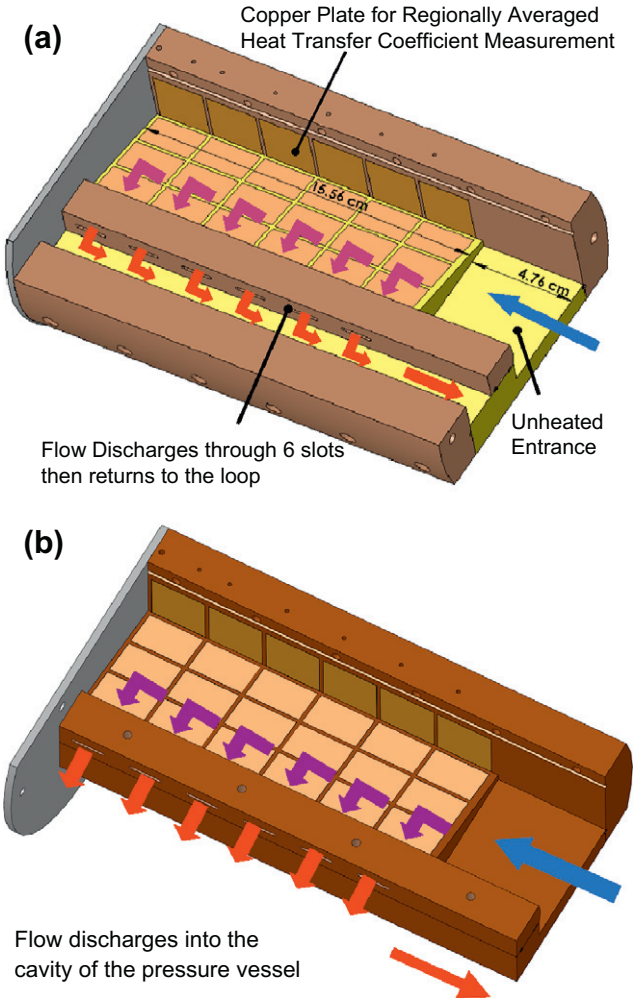

Fig. 3. Schematics of the wedge-shaped test section: (a) with cross flow effect from the discharged fluid in the return flow loop, and (b) without cross flow effect from the discharged fluid.

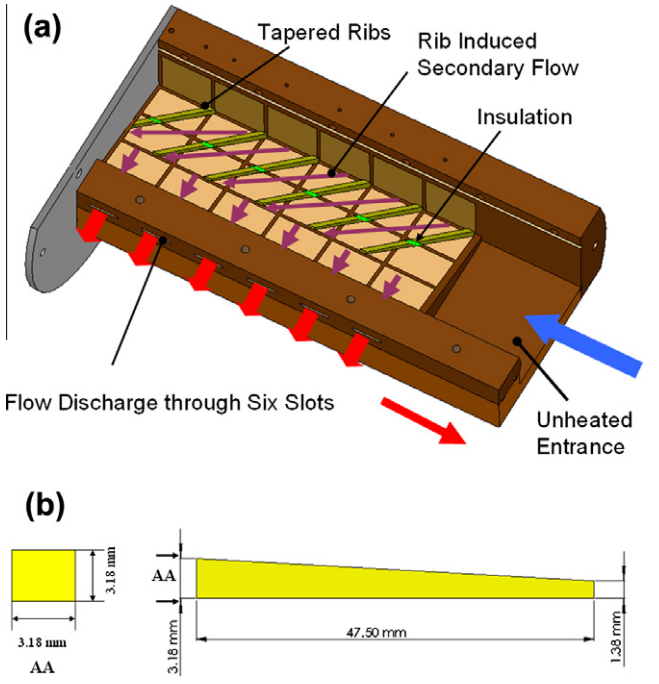

Fig. 4. (a) Wedge-shaped test section with ribs and (b) the dimensions of the tapered ribs of the current study.

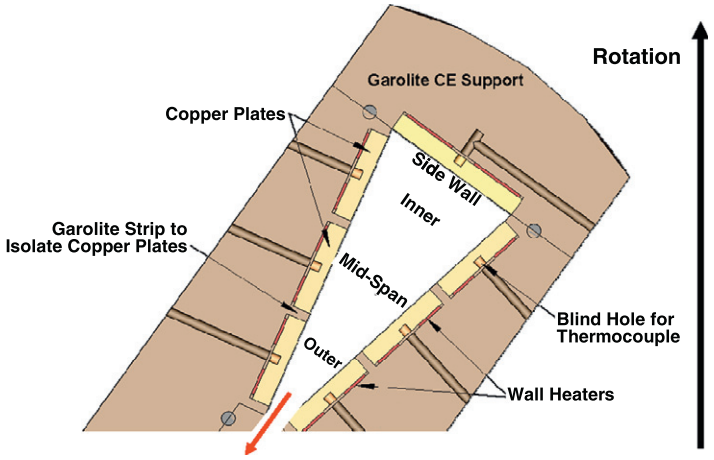

Fig. 5. Schematics of the wedge-shaped test section.

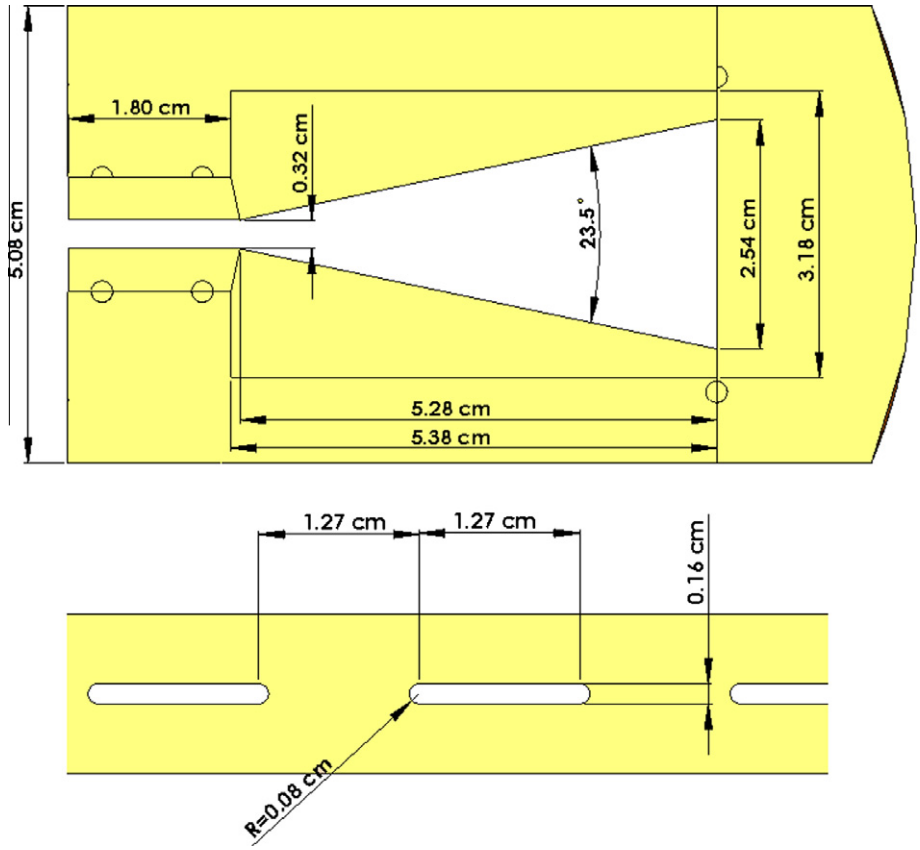

Fig. 6. Cross sectional view of the test section with slot.

3. Data reduction

3.1. Heat transfer measurement

The heat transfer coefficients can be determined from Newton's Law of Cooling as demonstrated in the following equation:

$$h = \frac{\dot{Q}_{net}}{A(T_{w,x} - T_{b,x})} = \frac{\dot{Q}_{in} - \dot{Q}_{loss}}{A(T_{w,x} - T_{b,x})} \quad (1)$$

The net rate of heat transfer is determined from the difference of the power supplied by each resistance heater and the heat lost from the test section. The heat losses are determined from a series of calibration tests during which insulation is filled into the entire channel to eliminate natural convection. Power is supplied by the heaters, and the power required to reach a series of given temperatures is recorded. The power supplied to the heaters during this calibration is equivalent to the heat lost during the actual measurement. Separate heat loss calibrations are required for each rotational speed.

The regionally averaged wall temperature ($T_{w,x}$) is measured using the thermocouple on each copper plate. With thermocouples placed at the inlet section and the exit of the last slot, the inlet and outlet bulk temperatures are known. The coolant bulk temperature

at a specific location ($T_{b,x}$) in the channel is determined based on linear interpolation between the measured inlet and outlet temperature. The Nusselt number ratio (Nu/Nu_0) demonstrated in Eq. (2) is used to determine the heat transfer enhancement level. Nu_0 is the Dittus–Boelter–McAdams correlation for fully developed turbulent flow in a smooth stationary tube.

$$\frac{Nu}{Nu_0} = \frac{hD_h/k}{0.023Re^{0.8}Pr^{0.4}} \tag{2}$$

3.2. Local mass flow rate measurement

The local mass flow rate decreases along the streamwise direction due to slot ejection from the wedge-shaped channel. The coolant flow remaining in the channel needs to be determined in order to obtain an accurate Nu_0. The estimated mass flow rate through the jth slot can be calculated by Eq. (3) from Kumaran et al. (1991).

$$\dot{m}_j = C_D A_j [2\rho(P_{in} - P_{exit})]^{1/2} \tag{3}$$

C_D is the discharge coefficient, and A_j is the cross-sectional area of the slot. The density is obtained by the pressure and bulk temperature at each location. Pressure taps at the inlet and exit of the slot were used to obtain the pressure drop, which is measured by a Dwyer inclined manometer. The total inlet mass flow is equal to the summation of the mass flow through each slot because all the coolant flows through slots. By assuming the discharge coefficients through these six slots are identical and the effect of rotation on it is the same, the mass flow rate through each slot therefore can be determined based on the conservation of mass. The local Reynolds number decreases as the flow goes downstream due to flow discharging through the slots as shown in Fig. 7. The local Reynolds numbers for both the smooth and ribbed cases are presented. It shows that the local Reynolds number distributions are very similar for all the cases. The local mass flow distribution is affected by the slot ejection; however, neither ribs nor rotation has significant effects on it.

The local rotation number is the ratio of the Coriolis force to the bulk flow inertia force. The rotation number is defined in the following equation:

$$Ro_x = \frac{\Omega D_h}{V_x} \tag{4}$$

This non-dimensional parameter is commonly used to quantify the effect of rotation by engineers in industry and academia. By varying the rotational speed (Coriolis force) and the Reynolds number (flow inertia force), the contribution from these two factors should yield the same results.

The buoyancy parameter is also a widely used non-dimensional parameter useful for quantifying the effect of rotation inside the gas turbine blade. The buoyancy force, due to the centrifugal force and temperature difference, plays a critical role in heat transfer distributions because of the high rotational speeds and large temperature gradients encountered in actual engines. The buoyancy parameter considers all factors including the density ratio (temperature difference), the rotation number, and the rotating radius. The local buoyancy parameter is shown in the following equation:

$$Bo_x = \left(\frac{\Delta\rho}{\rho}\right)_x (Ro_x)^2 \frac{R_x}{D_h} = \frac{T_{w,x} - T_{b,x}}{T_{f,x}} (Ro_x)^2 \frac{R_x}{D_h} \tag{5}$$

The film temperature ($T_{f,x}$) is defined as the average of the wall temperature and the bulk temperature. A density ratio of 0.11 was maintained for all the tests.

The uncertainty analysis is based on the method prescribed by Kline and McClintock (1953). In this wedge-shaped channel, the largest uncertainty occurs in the measured quantities at the inlet Reynolds number of 10,000. The overall uncertainty in the Nusselt

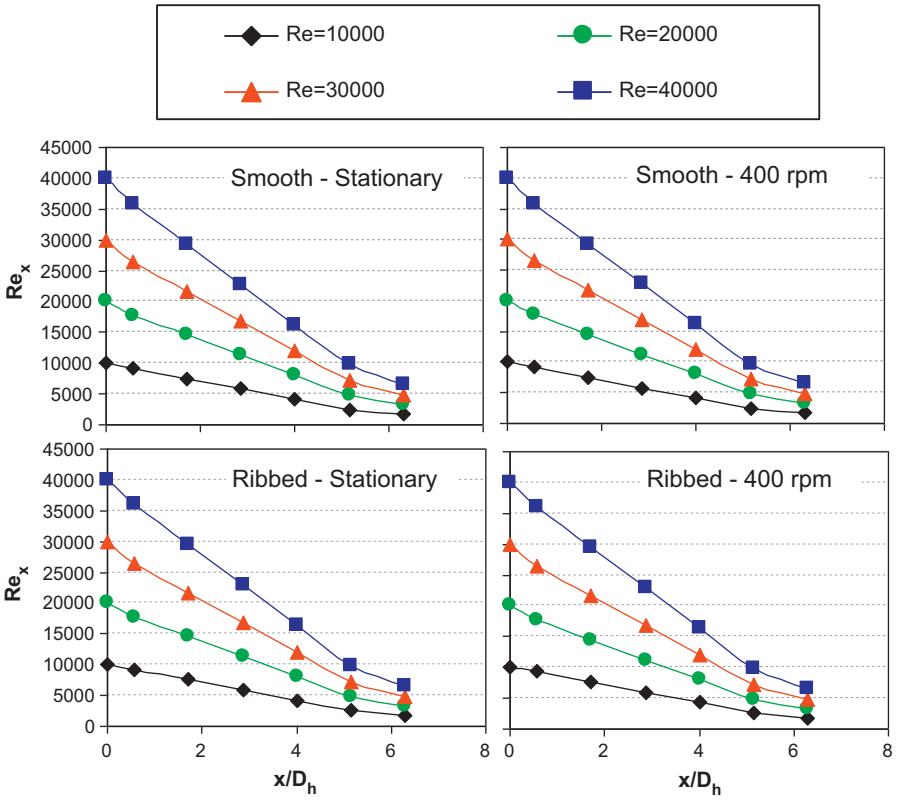

Fig. 7. Local Reynolds number distribution inside the channel.

number ratio is approximately 16.9% of the presented values. However, the overall uncertainty in the Nusselt number ratio decreases to approximately 5.8% of the calculated value at the highest inlet Reynolds number of 40,000.

4. Results and discussion

4.1. Effects of cross flow on pressure drop, mass flow, and heat transfer distribution

Mass flow through the slot is driven by the pressure gradient, which is influenced by the flow conditions with/without cross flow effect. Fig. 8 shows the pressure drop and mass flux ($G_j = \rho V_j$) across each slot at four different inlet Reynolds numbers. For the previous case (a), it shows that pressure drop is the highest at small x/D_h locations and is reduced along the streamwise direction. Higher Reynolds number shows a higher pressure drop, resulting in higher mass flux through the slot. Near the upstream region of the channel, more mass exits through the slots than the downstream region as shown in Fig. 8. This mass flow distribution behavior, affected by the cross flow, has a similar trend as the one reported by Huang et al. (1998). In the current study of case (b), the cross flow effect is eliminated by ejecting the jets into a large plenum. The pressure drop at each slot is more uniformly distributed. The mass flux is also more uniformly distributed as compared to the cross flow case (a). It is found that for both case (a) and (b), rotation did not have significant effects on the pressure drop and mass flux distribution. Fig. 9 shows the stationary Nusselt number comparisons of both cases at two different Reynolds numbers. Each point is the average of leading and trailing surfaces. At Re_i = 10,000, there is no significant difference between these two cases near the slot (outer and mid-span). At the regions away from the slots (inner and side wall), case (b) has higher Nusselt number values than case (a). When the inlet Reynolds number increases from 10,000 to 30,000, case (b) has higher Nusselt numbers in every region but the trend is similar to case (a).

4.2. Stationary results

Fig. 10 shows the Nusselt number inside the stationary channel with smooth and ribbed surface conditions. The local mass flow rate decreases along the streamwise direction due to slot ejection and the local Reynolds numbers are labeled on the first point and last point of the figure. Heat transfer is enhanced near the entrance for all the cases due to sudden contraction entrance effects. On the outer region, Nusselt number maintains the same level along the streamwise direction. The Nusselt number is 120 at a Reynolds number of 10,000 and is 200 at a Reynolds number of 30,000. It has the highest heat transfer level over the entire channel because it is close to the slot ejection region. Slot ejection not only alters turbulent mixing but also produces turning effects from mainstream flow to the exit jet. This also shows that the slot ejection can enhance heat transfer even for the low Reynolds number regions downstream. The other regions (mid-span, inner, and side wall) show that the Nusselt number decreases along the streamwise direction due to decreasing Reynolds number and the boundary layer development. The Nusselt number distribution decreases in the spanwise direction from the outer region of the channel to

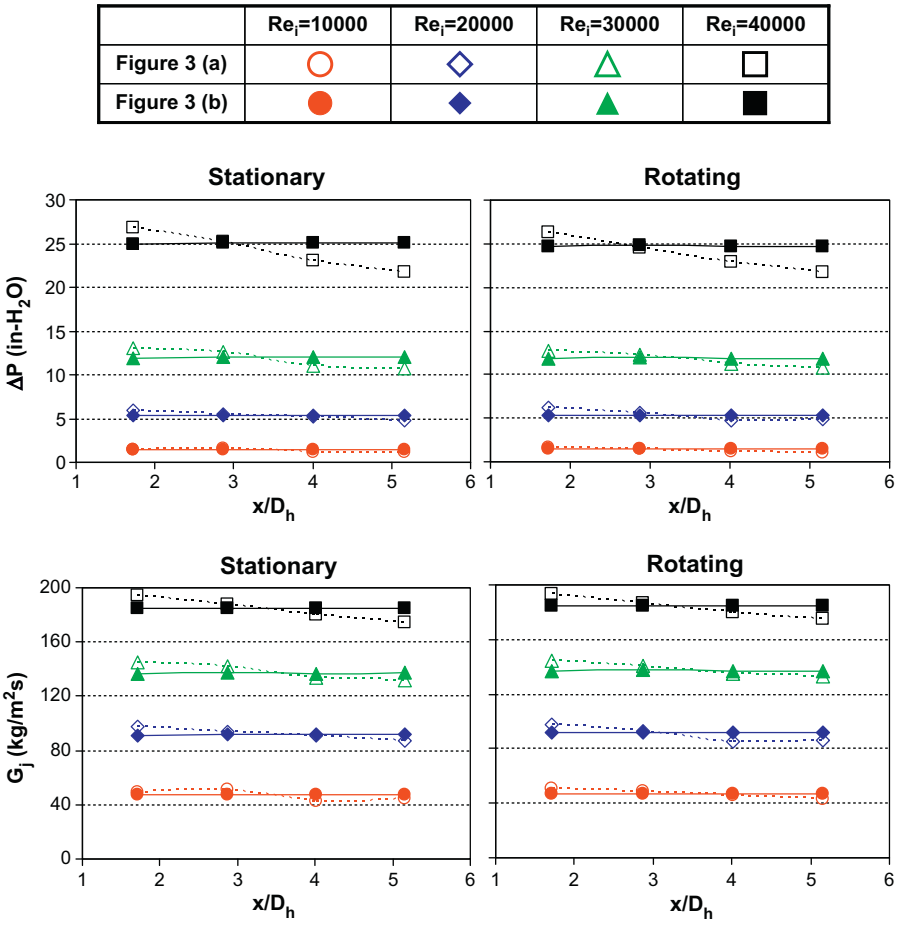

Fig. 8. Comparisons of pressure drop and mass flux across the slots with and without cross flow effect.

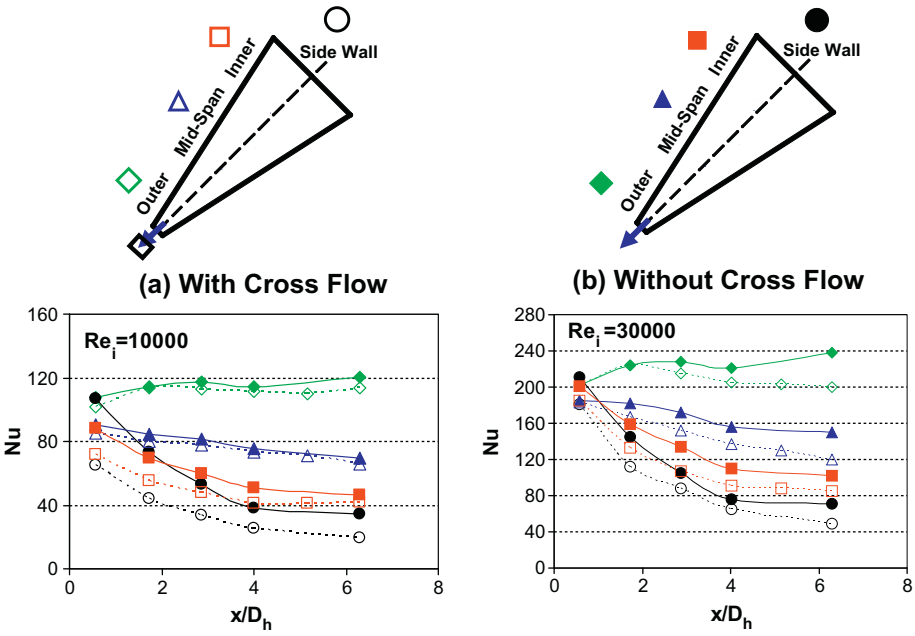

Fig. 9. Stationary Nusselt number comparison with and without cross flow.

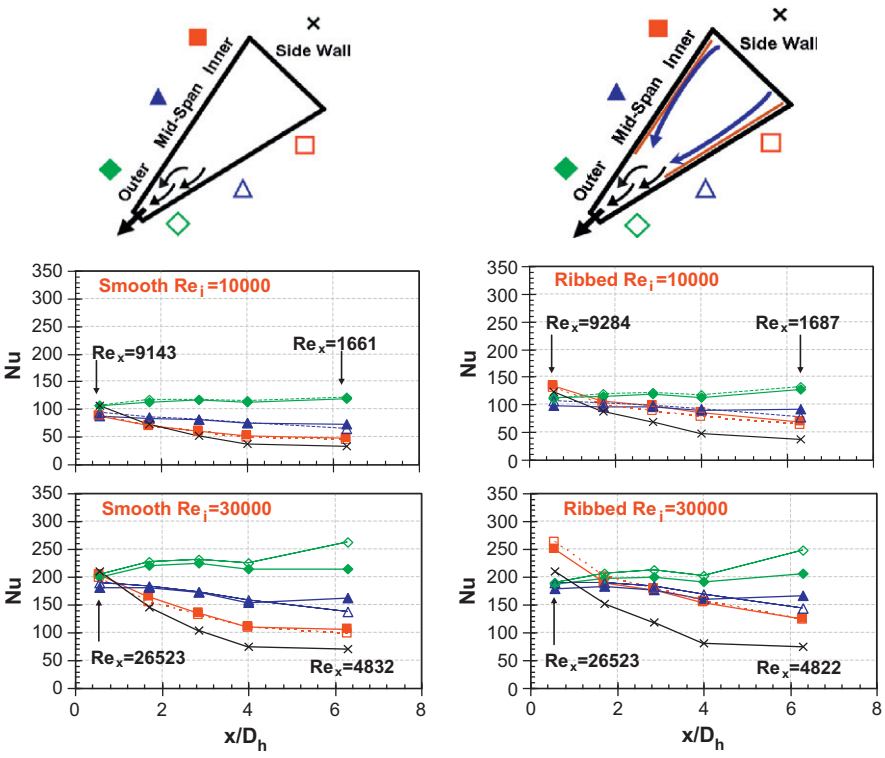

Fig. 10. Nusselt number distribution in the stationary channel.

the side wall due to decreased effects of slot ejection. Slot ejection has minor effects near the side wall and heat transfer is the lowest due to a thicker boundary layer. The Nusselt number decreases from 110 to 35 at Re_i = 10,000 and decreases from 200 to 75 at Re_i = 30,000 along the streamwise direction on the side wall region. As the Reynolds number increases, the Nusslet number also increases for all the regions.

From the above smooth case, heat transfer improvement is needed on the regions away from the slots. The ribs are put on the mid-span and inner regions to enhance heat transfer. 45° angled rib is chosen because generally angled ribs have better performance than orthogonal ribs. There is no rib on the outer region because the slot ejection already enhances heat transfer tremendously. The rib induced secondary flow progresses from the inner region towards outer region. Heat transfer enhancement is higher near the inner region compared to the mid-span region. The rib induced secondary flow tends to continue towards the outer region due to strong slot ejection. The heat transfer level is enhanced

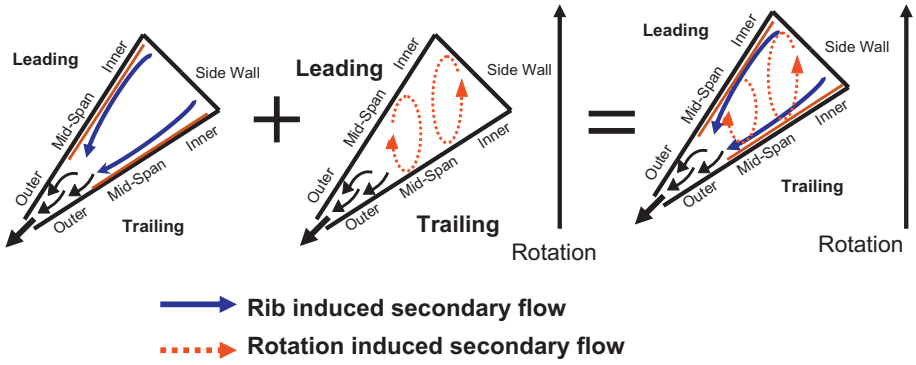

Fig. 11. Secondary flow induced by the rotation and ribs.

due to ribs but the trend is similar to the smooth case. On the inner region, the Nusselt number decreases along the streamwise direction from 130 to 70 at a Reynolds number of 10,000 and from 250 to 130 at a Reynolds number of 30,000. The Nusselt numbers are higher compared to the smooth case. It is noted that near the entrance region (x/D_h = 0.6), inner region has the highest heat transfer due to entrance effects in the ribbed channel. The heat transfer augmentation due to the ribs is reduced downstream because the mass flow remaining in the channel is decreasing. The heat transfer enhancement on the mid-span is smaller than the inner region. Highest heat transfer still occurs on the outer region as flow goes downstream for the ribbed case. There is no significant difference between the ribbed case and the smooth case on the outer region and side wall. The results show that even with the help from the ribs, inner and mid-span regions still have lower heat transfer than the outer region. Slot ejection has higher heat transfer enhancement than ribs in this channel.

4.3. Rotating results

When the channel is rotating, heat transfer is affected by the rotation induced Coriolis force and the rotational buoyancy force. A pair of counter rotating vortices is formed inside the rotating channel due to Coriolis force. The structure of the rotation induced vortices, with radially outward flow, as is the case in the current channel, is conceptually shown in Fig. 11. The effect of rotation is more obvious near the mid-span and inner region and diminishes towards the outer region. There is no clear rotating vortex structure near the outer region due to strong turbulent mixing caused by the slot ejection. Therefore, the effect of rotation is minor near the narrow region. With the channel orientation of 135°, heat transfer is enhanced on the trailing surface. The Nusselt number distribution in the rotating smooth channel is shown in Fig. 12. On the inner region, the effect of rotation is most obvious because the larger space allows counter rotating vortices to develop freely.

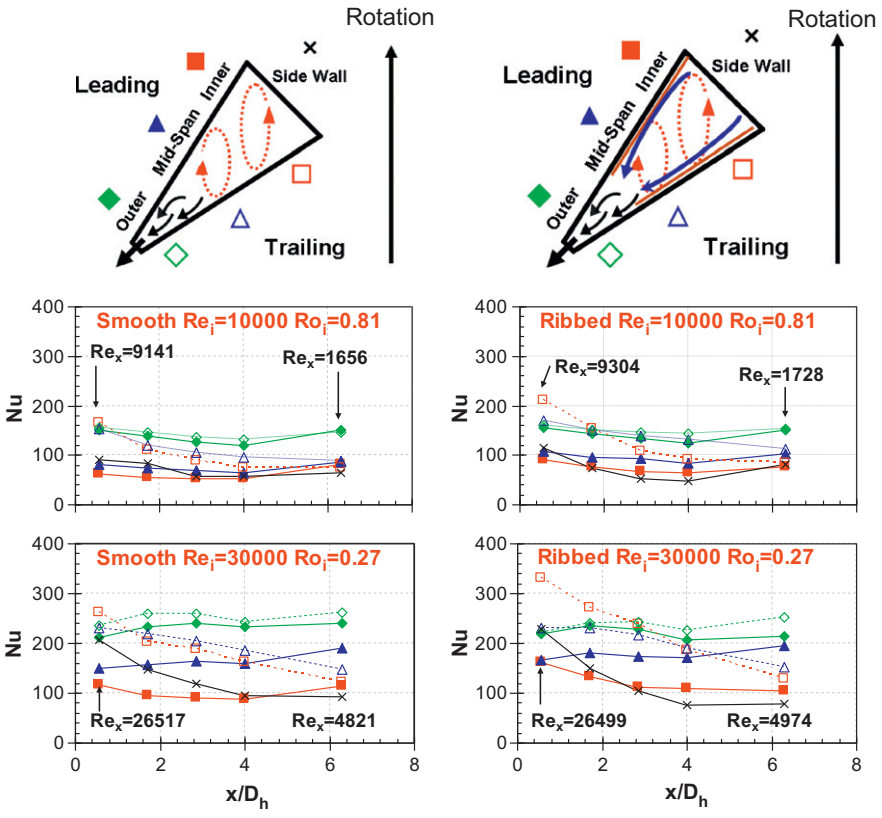

Fig. 12. Nusselt number distribution in the rotating channel.

The Nusselt number on the trailing surface is much higher than the leading surface in this region. The difference between leading and trailing surface is the largest, especially near the entrance region. Heat transfer is the lowest on the leading inner region when $x/D_h < 4.0$ and on the side wall when $x/D_h = 6.3$. The Nusselt number on the trailing surface is about 2.5 times higher than the leading surface at the entrance of the inner region. The difference between the leading and trailing surfaces reduces as flow progresses downstream. On the mid-span region, the trend is similar to the inner region. However, the difference between the leading and trailing surfaces is smaller due to smaller effect of rotation. The Nusselt number on the trailing surface is 1.5 times higher than the leading surface near the entrance of the mid-span region. The Nusselt number on the leading and trailing surfaces also converges as flow progresses downstream. On the outer surface, heat transfer on the trailing surface is only slightly higher than the leading surface. The strong slot ejection effect dominates over the effect of rotation and heat transfer is altered due to rotation on both surfaces. From Fig. 8, it can be observed that the measured mass flux through each slot is almost identical. The Nusselt number on this outer region shows almost the same value along the streamwise direction due to the same mass flux through slots.

For the ribbed case, the ribs also induced secondary flow inside this channel. With the ribs put on the leading and trailing surfaces, the heat transfer distribution is affected by the combined effects from rib and rotation. The Nusselt number distribution for the rotating ribbed channel is also shown in Fig. 12. The Nusselt number is the lowest either on the leading inner region or the side-wall. On the inner region, heat transfer also enhanced on the trailing surface. The Nusselt number on the trailing surface is 2.1 times higher than the leading surface at entrance. The Nusselt number difference between leading and trailing surface becomes smaller as flow progresses downstream. Similar trends can also be observed on the mid-span region while the heat transfer is enhanced compared to the smooth rotating case. Highest heat transfer also occurs on the outer region. It shows that neither the rib nor rotation has significant effects on heat transfer because of the strong slot ejection on the outer region. It is seen that rotation has larger enhancement near the entrance and effect of rotation is minor near the downstream region.

4.4. Rotation number effects

In order to study the heat transfer enhancement due to rotation, the ratio of the rotating Nusselt number to the stationary Nusselt number (Nu/Nu_s) has been plotted with the local rotation number. The local rotation number is determined by the local velocity in each region. Results in the smooth channel from two different regions (2 and 4) along the streamwise direction ($x/D_h = 1.7$ and 4.0) are reported in Fig. 13. Reynolds number effects have been eliminated and all the data points can be correlated into a single curve. The discussion starts with region 2 which is near the entry region of this duct. Highest heat transfer enhancement due to rotation occurs on the trailing surface of the inner wall where the Nusselt number is 1.6 times higher than the stationary case. On the leading surface of the inner wall, Nu ratio decreases until

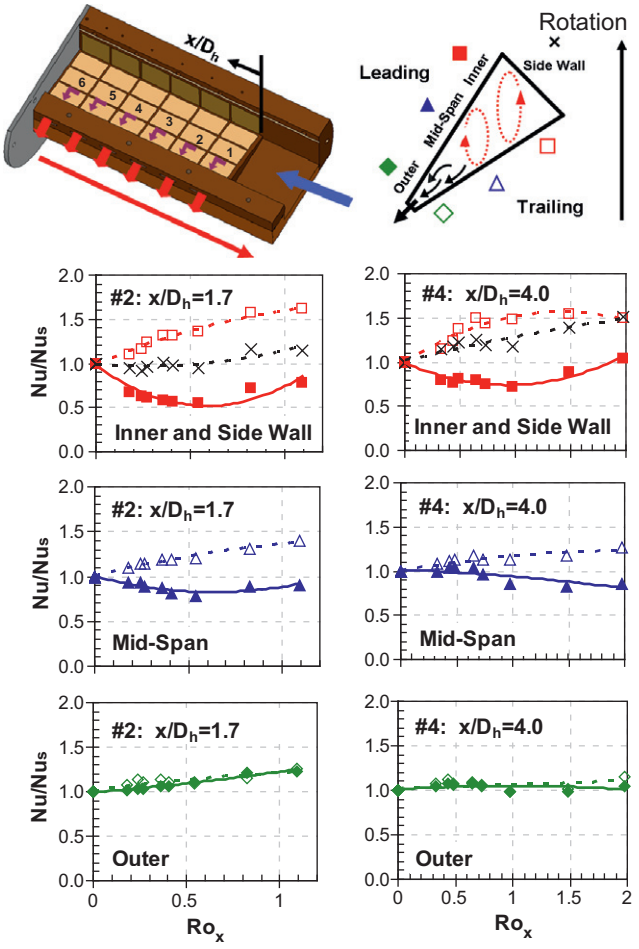

Fig. 13. Effect of local rotation number on nusselt number ratios in the smooth channel (Nu/Nu_s) for all the inlet Reynolds numbers (Re_i = 10,000–40,000).

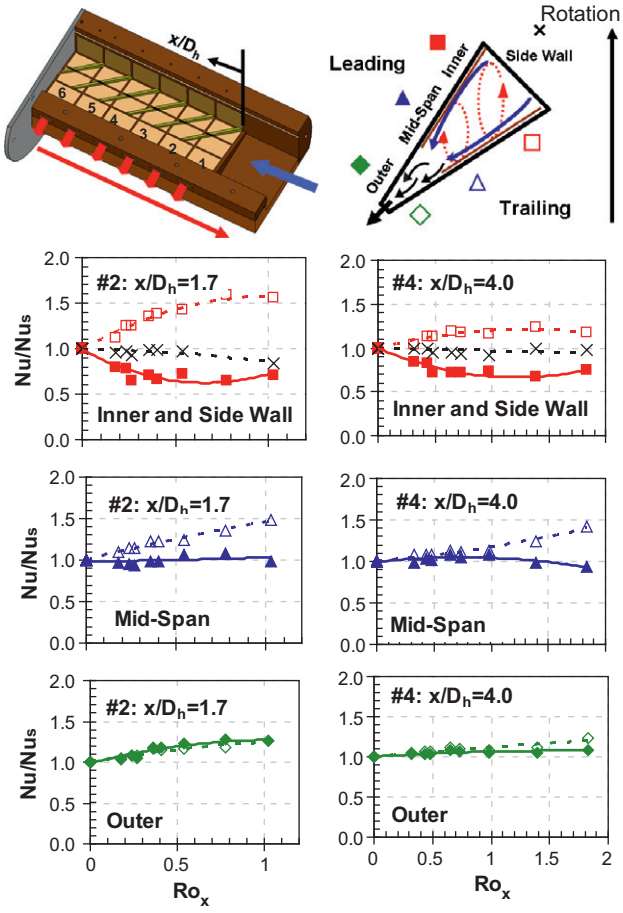

Fig. 14. Effect of local rotation number on Nusselt number ratios in the ribbed channel (Nu/Nu_s) for all the inlet Reynolds numbers (Re_i = 10,000–40,000).

a rotation number of 0.55, and then increase with an increase of rotation number. Rotation results in the decreasing of heat transfer in this region. For the side wall, it gradually increases with rotation number but the heat transfer enhancement due to rotation is smaller than the inner trailing surface. In the mid-span region, it shows that effect of rotation also enhances heat transfer on the trailing surface but decreases heat transfer on the leading surface. Near the outer region, results are affected by the combined effects of ejection and rotation. It shows that Nu ratios on the leading and trailing surfaces are similar and both increase with rotation number. Similar trends can be observed in region 4. The difference between the leading and trailing surface decreases from the inner region towards the outer region for both region 2 and region 4. The Nusselt number ratio (Nu/Nu_s) distribution with rotation number for the ribbed surface is plotted in Fig. 14. It shows comparable trends to the smooth case while heat transfer enhancement/degradation level is altered due to influence of ribs near the inner and mid-span region. It is noted that for the side wall, Nu ratio maintains the same level as rotation number increases. Results from smooth case and ribbed case are almost identical in the outer region, indicating profound effect of slot ejection in this region.

4.5. Average heat transfer

The average heat transfer enhancements on the leading and trailing surfaces are averaged over the inner, mid-span, and outer regions. Each data point is the average of 18 pints on the leading (or trailing) surface and the average of six points on the side wall. The averaged Nusselt number ratios (Nu/Nu_0) are shown in Fig. 15. The average rotation number and average buoyancy parameter are also the average of the local values from each region. It has been established that the heat transfer enhancement varies across the entire channel. Over the range of Reynolds numbers and rotational speeds, all the data points of these three surfaces can be fitted into a single curve. Most notably, the Nusselt number ratios increase as the rotation number and buoyancy parameter increases for all three surfaces. The correlations have been generated as a function of the rotation number (Ro) as shown in Eq. (6) as well as the buoyancy parameter (Bo) as shown in Eq. (7):

$$Nu/Nu_0 = A \cdot Ro^m + B \cdot Ro^n \quad (6)$$

$$Nu/Nu_0 = A \cdot Bo^m + B \cdot Bo^n \quad (7)$$

The constants for the above correlation functions are listed in Table 1. The maximum discrepancies are within ±12% for the smooth case and ±10% for the ribbed case. These correlations show that the heat transfer enhancement can be predicted by the rotation number and buoyancy parameter in this wedge-shaped channel with either smooth surface or ribbed surface.

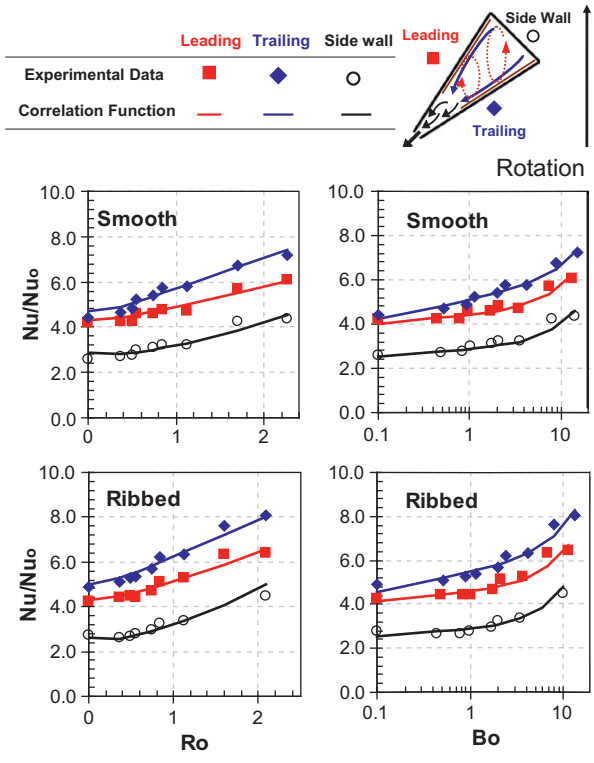

Fig. 15. Correlations for heat transfer enhancement with average rotation number and buoyancy parameter for all the inlet Reynolds numbers (Re_i = 10,000–40,000).

Table 1
Correlation coefficients for Nu ratio in wedge channel.

Ro	A	B	m	n
Smooth				
Leading	0.8	4.1	1.1	−0.01
Trailing	1.4	4.3	1	−0.02
Side wall	0.6	2.6	1.45	−0.02
Ribbed				
Leading	1.02	4.1	1.2	−0.01
Trailing	1.7	4.55	1	−0.02
Side wall	0.9	2.3	1.5	−0.03
Bo	A	B	m	n
Smooth				
Leading	4.4	0.025	0.04	1.55
Trailing	5.1	0.01	0.08	1.7
Side wall	2.85	0.025	0.05	1.51
Ribbed				
Leading	4.56	0.04	0.04	1.55
Trailing	5.45	0.02	0.08	1.7
Side wall	2.85	0.05	0.05	1.51

5. Conclusion

Heat transfer has been experimentally measured inside a wedge-shaped channel to simulate the trailing edge of the gas turbine blade. Smooth surface as well as the 45° ribbed surface was tested to see the heat transfer enhancement. Tapered ribs were used to improve the low heat transfer regions away from the slots. The coolant has been discharged through six slots and the local mass flow remaining in the channel has been determined. Effect of cross flow on pressure drop, mass flow, and heat transfer was investigated. The experiments were conducted under high rotation number and high buoyancy parameter to simulate the actual engine condition. The following conclusions can be drawn:

1. Effect of cross flow gives higher pressure drop and mass flow at upstream regions; while in the current study they are distributed more uniformly under no cross flow condition.
2. Based on the stationary results, Nusselt number is the highest near the narrow region due to slot ejection for both smooth and ribbed cases. Heat transfer decreased towards the wide region of the channel due to reduced slot ejection effect. Tapered ribs enhance heat transfer on the ribbed surface but still lower than the region with ejection.
3. Heat transfer enhancement/degradation due to rotation is stronger near the wider region (inner) than the narrow region (outer). Effect of slot ejection dominates and the heat transfer enhancement (Nu/Nu_s) gradually increases with rotation near the narrow region.

4. Both the rotation number and buoyancy parameter can be correlated to predict heat transfer enhancements for the smooth case and ribbed case in the extended range.

Acknowledgment

This work has been funded through Marcus Easterling Endowment Fund.

References

Carcasci, C., Facchini, B., Innocenti, L., 2003, Heat Transfer and Pressure Drop Evaluation in Thin Wedge-Shaped Trailing Edge, ASME Paper No. GT2003-38197.

Chang, S.W., Liou, T.M., Chiou, S.F., Chang, S.F., 2008. Heat transfer in high-speed rotating trapezoidal duct with rib-roughened surfaces and air bleeds from the wall on the apical side. ASME J. Heat Transfer 130, 061702-1–061702-13.

Cunha, F.J., Chyu, M.K., 2006. Trailing-edge cooling for gas turbines. J. Propul. Power 22 (2), 286–300.

Dutta, S., Han, J.C., Lee, C.P., 1996. Local heat transfer in a rotating two-pass ribbed triangular duct with two model orientations. Int. J. Heat Mass Transfer 39, 707–715.

Griffith, T.S., Al-Hadhrami, L., Han, J.C., 2002. Heat transfer in rotating rectangular cooling channels (AR = 4) with angled ribs. ASME J. Heat Transfer 124, 617–625.

Han, J.C., Dutta, S., Ekkad, S.V., 2000. Gas Turbine Heat Transfer and Cooling Technology. Taylor and Francis, New York.

Huang, Y., Ekkad, S.V., Han, J.C., 1998. Detailed heat transfer distributions under an array of orthogonal impinging jets. AIAA J. Thermophys. Heat Transfer 12 (1), 73–79.

Hwang, J.J., Lu, C.C., 2001. Lateral-flow effect on endwall heat transfer and pressure drop in a pin fin trapezoidal duct with various pin shapes. ASME J. Turbomach. 123, 133–139.

Johnson, B.V., Wagner, J.H., Steuber, G.D., Yeh, F.C., 1994. Heat transfer in rotating serpentine passage with selected model orientations for smooth or skewed trip walls. ASME J. Turbomachinery 116, 738–744.

Kline, S.J., McClintock, F.A., 1953. Describing uncertainty in single-sample experiments. Mech. Eng. 75, 3–8.

Kumaran, T.K., Han, J.C., Lau, S.C., 1991. Augmented heat transfer in a pin fin channel with short or long ejection holes. Int. J. Heat Mass Transfer 34 (10), 2617–2628.

Lau, S.C., Han, J.C., Kim, Y.S., 1989a. Turbulent heat transfer and friction in pin fin channels with lateral flow ejection. ASME J. Heat Transfer 111, 51–58.

Lau, S.C., Han, J.C., Batten, T., 1989b. Heat transfer, pressure drop, and mass flow rate in pin fin channels with long and short trailing edge ejection holes. ASME J. Heat Transfer 111, 116–123.

Liou, T.M., Chang, S.W., Hung, J.H., Chiou, S.F., 2007. High rotation number heat transfer of 45 rib-roughened rectangular duct with two channel orientations. Int. J. Heat Mass Transfer 50, 4063–4078.

Liu, Y.H., Huh, M., Wright, L.M., Han, J.C., 2008. Heat transfer in trailing edge channels with slot ejection under high rotation numbers. AIAA J. Thermophys. Heat Transfer 23 (2), 305–315.

Taslim, M.E., Li, T., Spring, S.D., 1995. Experimental study of the effects of bleed holes on heat transfer and pressure drop in trapezoidal passages with tapered turbulators. ASME J. Turbomach. 117, 281–289.

Wagner, J.H., Johnson, B.V., Hajek, T.J., 1991. Heat transfer in rotating passage with smooth walls and radial outward flow. ASME J. Turbomach. 113, 42–51.

Wright, L.M., Lee, E., Han, J.C., 2004. Effect of rotation on heat transfer in rectangular channels with pin fins. AIAA J. Thermophys. Heat Transfer 18 (2), 262–272.

Wright, L.M., Liu, Y.H., Han, J.C., Chopra, S., 2008. Heat transfer in trailing edge, wedge-shaped cooling channels under high rotation numbers. ASME J. Heat Transfer 130 (7), 071701-1–071701-11.

Zhou, F., Lagrone, J., Acharya, S., 2004. Internal Cooling in 4:1 AR Passages at High Rotation Numbers, ASME Paper No. GT 2004-53501.